



Mitigating internal shorting to enhance battery safety with gradient-conductivity cathodes

Matthew S. Gonzalez, Zhaohui Wu, John Holoubek, Qizhang Yan, Haodong Liu, Ping Liu*

Department of Nanoengineering, University of California San Diego, 9500 Gilman Drive, La Jolla, CA, 92093, United States

HIGHLIGHTS

- Electrode with gradient conductivity mitigates thermal runaway due to shorting.
- Electrode fabricated by selectively removing conductive carbon from the surface.
- The increased short circuit resistance reduces current and temperature rise.
- Battery performance remains unaltered until a shorting event.

ARTICLE INFO

Keywords:

Lithium metal battery
Dendrite interception
Battery safety
Internal short circuit
Etching

ABSTRACT

Internal short circuits and the resulting catastrophic battery failure is difficult to detect and can occur under normal working conditions. To enable future high-energy density batteries, particularly lithium metal, an inexpensive internal short protection scheme is required. Here, we selectively remove conductive carbon from the cathode surface, creating a gradient-conductivity electrode. The process etches to a depth of only 5–10 μm and the active particles maintain electrical contact through the backside allowing for otherwise unaltered battery performance. When a lithium dendrite contacts the cathode surface, it will react with the oxide particle rather than contacting the carbon network. The active material now acts as a resistive element limiting the current. During shorting tests induced by abuse charging, cells containing conductivity-gradient cathodes saw a 2x reduction in short circuit current and accompanying temperature rise compared to cells with uniform conductivity cathodes. The reduction in short circuit current thus renders the event harmless. Postmortem analysis shows the dendrites only contact the surface oxide particles, supporting the viability of this gradient conductivity electrode design. Our approach utilizes the intrinsic resistivity of the active material to improve battery safety, is broadly applicable, and incurs no penalty in energy density.

1. Introduction

In response to the need of portable electronics and electric vehicles, the energy densities of lithium-ion batteries have continued to rise. In the near term, reduction of inactive materials has proven to be successful. The thickness of commercial battery separators has been reduced to $<10 \mu\text{m}$ [1], while electrode areal specific capacity [mAh/cm^2] continue to rise [2]. In the long-term, the graphite anode will be replaced by higher capacity electrode materials, namely silicon containing materials [3] and ultimately lithium metal [4].

These changes in design and materials make battery safety an increasingly difficult challenge [5]. For LIBs, it is well known that

mechanical deformation [6] and overcharging [7] can induce internal shorting and dangerous thermal runaway. However, this can also occur without discernible external cause while operating under normal conditions [8,9]. The suspected cause of these type of events is a failure of the separator creating a low *electronic resistance* internal short circuit within the battery [10]. The challenge of separator failure further increases with the use of lithium metal anodes, especially during rapid charging when the likelihood of Li dendrite penetration increases [11].

Approaches to improve battery safety generally add a protective element within the battery to block, drain, or cut off the short circuit. Battery separators play an essential role in this function. The addition of various porous polymer layers [12], non-woven mats [13], or ceramic

* Corresponding author.

E-mail address: piliu@eng.ucsd.edu (P. Liu).

<https://doi.org/10.1016/j.jpowsour.2021.230412>

Received 7 July 2021; Received in revised form 17 August 2021; Accepted 18 August 2021

Available online 1 September 2021

0378-7753/© 2021 Elsevier B.V. All rights reserved.

coatings [14] have shown improvement of mechanical properties over standard polyolefin separators and aid to physically block dendrite propagation. All ceramic solid ion conductors acting as both separator and electrolyte can also suppress dendritic growth [15]. Materials can be added within the separator that are reactive towards Li and serve to etch away oncoming dendrites, but are limited by the material capacity past which dendrite propagation begins again [16]. Similarly, third electrodes sandwiched in the separator have been implemented to detect dendrite penetration and diagnose the health of the cell [17]. Most commonly battery separators are designed with an additional layer of porous material that undergoes a phase transformation and pore collapse at elevated temperature to cut off the ionic pathway and suspend shorting—ideally accomplished before thermal runaway initiates [18].

Another approach beyond modifying the separator is to break the electronic pathways within the electrodes themselves to limit the impact of shorting. Several methods have been developed to electronically isolate the active material. Current collectors have been designed to fracture upon mechanical deformation limiting self-discharge to small, isolated regions [19]. Positive thermal coefficient (PTC) materials have also been coated on the current collector or on the cathode itself to insulate the active material from the current collector or each other upon reaching elevated temperatures [20–22]. Unlike these temperature-triggered methods, we have recently introduced a partially electronically conductive (PEC) Janus separator to intercept oncoming dendrites. The PEC layer, in contact with the cathode, is permeable to lithium ions but adds electronic resistance to the short circuit formed when a dendrite makes contact, thus limiting the internal short-circuiting current and the temperature rise, rendering the short practically harmless [23].

All of these protection schemes, whether separator or electrode based, involve adding a component to the battery which invariably incurs increased manufacturing costs, adds to the overall volume, and increases the electronic or ionic resistance of the battery. In order for a protection scheme to be not only effective, but also economically scalable, it should ideally utilize the intrinsic properties of the electrode materials and architecture without incurring penalties in cell volume, weight, or resistance.

2. Results and discussion

2.1. Gradient-conductivity cathodes

Here we introduce a method to achieve increased electronic resistance for a short circuit by using a cathode material with a gradient electronic conductivity. Specifically, a reduced electronic conductive (REC) layer is created in the top layer of the cathode facing the separator side. In a common cathode (Fig. 1b), the active material, usually a metal oxide, is mixed with carbon to increase the electronic conductivity and held together by a polymer binder. If a dendrite contacts the conductive carbon network then the entire cathode is effectively shorted to the anode which can result in rapid self-discharge, Joule heating, and thermal runaway. In contrast, Fig. 1a shows a schematic of the REC interlayer, where the cathode's conductive carbon network has been selectively etched away from the cathode surface. When a dendrite shorts the anode and cathode, the short circuit must travel through the layer of the carbon-free active material. Common transition metal oxides cathode materials have low electronic conductivity ($10^{-3} - 10^{-8}$ S/m) [24–26], and is the very reason conductive carbon is required to achieve good cycling performance at even low C-rates [27]. In the absence of carbon, however, the active material acts as a convenient high resistance short circuit intercept. Additionally, since the etching is limited to the cathode surface, the bulk of cathode remains electronically connected, which should allow for unaltered cycling performance outside of a failure event.

To selectively etch the surface of the cathode a simple sputter etching technique was employed to remove the carbon species (conductive carbon and polymer binder) from the surface of the cathode without damaging the active material. By reversing the polarity in a laboratory sputtering deposition system, Ar^+ was generated to bombard the cathode and strip away surface materials. The cathodes used are high energy density commercial quality electrode tapes roughly 50 μm thick on Al foil. The active material is $\text{Li}_x\text{Ni}_{0.5}\text{Mn}_{0.3}\text{Ni}_{0.2}\text{O}_2$ (NMC), with PVDF as the binder, and MWCNTs as the conductive carbon network in a weight ratio of 97.5 : 1.5 : 1. It should be noted that this cathode tape was chosen to represent a generic commercially available battery cathode. Electrodes can be fabricated with differing thickness and particle composition and morphology, which might impact the optimum etching condition to achieve the desired safety enhancement effect but the process itself is generally applicable. Fig. 2 shows high magnification SEM images of cathode surfaces that underwent a) 30-min, b) 10-min,

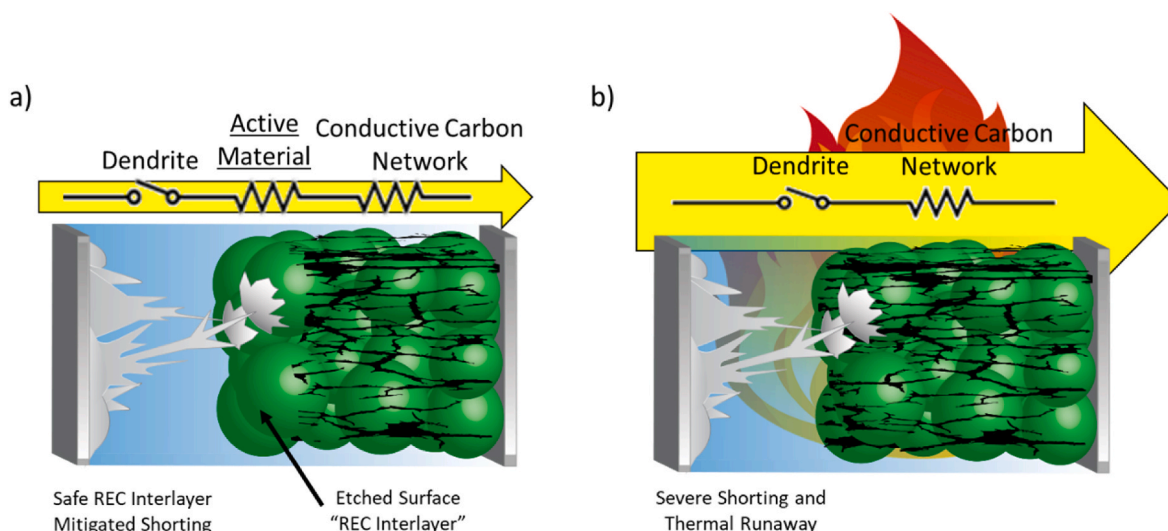


Fig. 1. Working mechanism of internal short mitigation with a gradient conductivity cathode. **a)** schematic of an etched cathode where the surface carbon is removed and the active material adds an additional resistive element to the short circuit when a dendrite shorts the anode to the cathode. **b)** Schematic of an unetched pristine cathode where the conductive carbon and dendrite generates a low resistance short circuit and possible thermal runaway events.

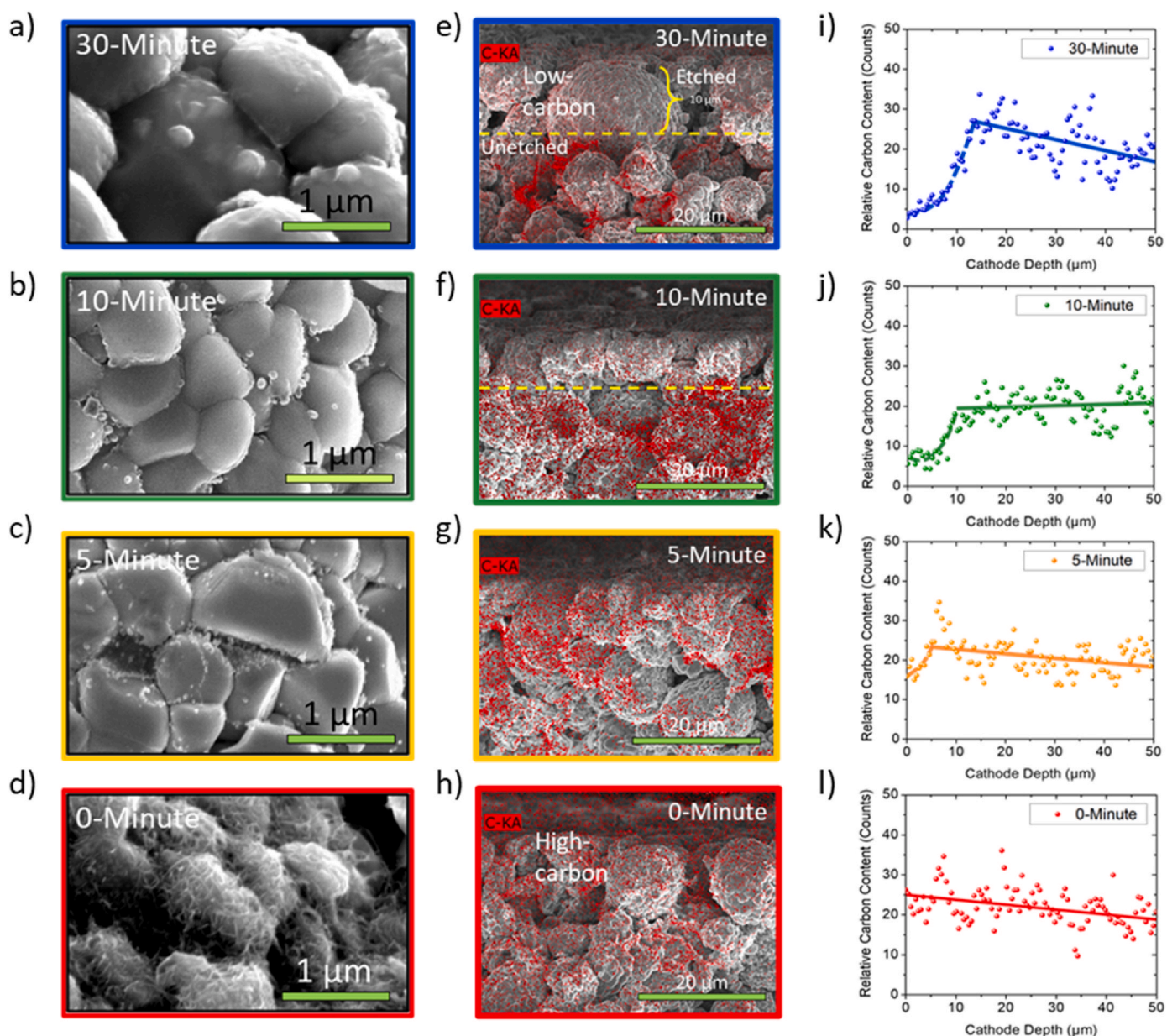


Fig. 2. Characterization of the conductivity gradient cathodes. High magnification SEM images of the cathode surface after etching for a) 30-min, b) 10-min, c) 5-min, and d) 0-min. Cross-section SEM titled by 5° focusing on the cathode surface and roughly 20 μm depth with EDS elemental mapping overlay of carbon element for cathodes etched for e) 30-min, f) 10-min, g) 5-min, and the h) pristine (0-min) cathode. i-l) The average relative carbon content collected by EDS line scan as a function of cathode depth for each etching time with linear fitting overlay for the unetched region and polynomial fit for the etched region.

and c) 5-min etching as well as a d) 0-min (pristine) electrode. While there is no obvious difference to the naked eye (Supporting Information, Fig. S1), SEM shows 30-, 10- and 5-min etching results in a smooth and carbon free NMC surface, while the pristine cathode has a clear mat of MWCNTs coating the surface giving it a fuzzy appearance.

Cross-sectional SEM images with EDS elemental mapping of carbon overlaid for electrodes after 30-min (Fig. 2e) and 10-min etching (Fig. 2f) show that carbon has been removed from a depth of roughly 10 μm into the cathode surface. Higher magnification SEM focusing a surface particle shows etching removes carbon from only the upper hemisphere of the particle where the lower hemisphere is shaded due to the line-of-sight nature of the sputter etching process (Supporting Information, Fig. S2). Due to only a minor difference between 30- and 10-min etched cathodes longer etching times were not considered. The 5-min etching (Fig. 2g), while sufficient to remove surface carbon, does not appear to penetrate meaningfully into the cathode. The pristine cathode

has carbon extending uniformly throughout the cathode including the surface (Fig. 2h). EDS line scans detecting C were performed at 20 individual cross-section locations along each cathode sample, these were averaged, fitted, and plotted in Fig. 2i. The 30- and 10-min etched cathodes again show little relative C signal until a depth of 10 μm where there is significant increase in C content. The C signal intensity plateaus at 4-5x the relative content detected on the surface and remains constant throughout the bulk. The 0-min (pristine) cathode shows the same relative carbon content that is constant from surface to bottom of the cathode, while the 5-min etching shows some removal of surface carbon but fails to penetrate past a depth of <5 μm . The overall slight downward trend in carbon content through the cathode depth is attributed to a blocking effect decreasing the amount of signal that reaches the EDS detector, and we expect the carbon is most likely constant throughout.

2.2. Electrical characterization

The change in the electronic conductivity due to removing the surface conductive carbon network was measured to correlate etching time with the expected increase in electronic resistance upon an internal short. The resistance measurement was conducted using four parallel copper stripes placed on freestanding sheets of various etched and unetched cathodes. We use the resistance for a given area (Ωcm^2) of the cathode to characterize the impact of etching and the results are summarized in Table 1. Note that after etching, the electrode is composed of the REC layer under which is the more conducting, pristine layer. The in-plane resistance is thus very sensitive to the REC layer thickness. Details of resistance calculation are provided in Supporting Information, Fig. S3. A continuous increase in resistance is observed as the etching time increases, from 45.1 Ωcm^2 for the 0-min etched to 203.5 Ωcm^2 for the 30-min etched cathode tape. The added through plane resistance from etching is approximately half of the increase over the 0-min etched sample using the in-plane method and was calculated to be 6.8 Ωcm^2 , 65.5 Ωcm^2 , and 79.2 Ωcm^2 for the 5-min, 10-min, and 30-min etched cathodes, respectively. Note that these are increases of electronic resistance for dry electrodes. As shown below, the battery performance under normal operating conditions is largely unaltered.

Additionally, a completely carbon-free cathode was also casted with only NMC and PVDF binder (97.5 : 2.5 wt%) to measure the conductivity of the NMC particles themselves. The resistance of this was determined to be $6.53 \times 10^3 \Omega\text{cm}^2$, and the conductivity σ was calculated to be $1.63 \times 10^{-5} \text{ S/m}$. This is a very large increase over $3.05 \times 10^0 \text{ S/m}$ measured for the pristine cathode tape containing carbon and highlights the need to incorporate a conductive network between the active materials. Furthermore, this carbon-free tape was lithiated by direct contact with Li metal to simulate the chemical state the NMC would be in at the immediate area of Li dendrite contact. This overlithiated state has a higher conductivity than the pristine carbon-free NMC, $1.26 \times 10^{-4} \text{ S/m}$ but is still orders of magnitude lower than that of the normal pristine cathode added with carbon. It is expected that the contact area in immediate contact with Li metal will be reduced to 0 V by the dendrite. Benedek et al. [28] proposed that LiMO_2 materials (where M is a transition metal) undergo a multi-step reduction upon overlithiation that ultimately result in the formation of a physical mixture of M^0 and Li_2O via a conversion reaction mechanism. The reaction resulted in a nearly 4-5x increase in cathode thickness (Supporting Information, Fig. S4). The observed higher electronic conductivity in this state compared to the unreacted carbon free tape is likely due to the reduction of the Ni, Mn, and Co to a fully metallic state; however, the other nonconductive product of Li_2O keeps the overall bulk conductivity several orders of magnitude lower than that of the conductive carbon network and should still provide sufficient electronic resistance in the event of a short.

SEM investigation of pristine and NMC secondary particles that have been overlithiated by direct contact with Li metal for 24 h show a clear volume expansion that pulverizes the secondary particles and cracks the primary particles (Supporting Information, Fig. S5). This overlithiated product was characterized by XRD to reveal a featureless spectrum when compared to the pristine NMC material (Supporting Information,

Table 1

Electrical area specific resistance of 0-min, 5-min, 10-min, and 30-min etched freestanding cathode tapes, the active material with no conductive carbon, and the active material with no conductive carbon after being overlithiated by direct contact with Li metal.

	Cathode Resistance (Ωcm^2)	Conductivity (S/m)
0-Minute Etched	45.1	3.05×10^0
5-Minute Etched	58.6	n/a
10-Minute Etched	176.0	n/a
30-Minute Etched	203.5	n/a
Carbon-Free	6.53×10^3	1.63×10^{-5}
Overlithiated Carbon-Free	n/a	1.26×10^{-4}

Fig. S6). It has previously been reported that similar overlithiation via the conversion reaction of LiCoO_2 material resulted in nanoscale metal domains that were smaller than the coherence of the X-rays, resulting in similar featureless spectra [29]. XPS of the samples show a clear redshift after overlithiation. The peaks positions of Ni at 852.5 eV, Mn at 639.6 eV, and Co at 776.6 eV (Supporting Information, Fig. S7) are consistent with what is generally reported for the metallic chemical state of these elements [30–32], and supports the hypothesis that nanodomains of metal Ni, Mn, and Co are mixed with nonconductive Li_2O .

2.3. Electrochemical characterization

While the etching process is not expected to damage the active material since oxides are generally more difficult to remove than carbon and polymer species [33], electrochemical cycling of the cathodes was carried out to ensure the etching process has no adverse effects on the cathode performance (Fig. 3). Tests were performed using Li metal as the anode and LP30 as the electrolyte (1 M LiPF_6 EC:DMC 1:1 wt%). There is no notable difference between any etched cathodes and the pristine (0-min etched) cathode during the formation cycle and the 3rd cycle (Fig. 3a) when cycled at a rate of C/10. Since the carbon network provides the necessary electronic conductivity to cycle at high current densities, the cathodes were tested at rates of C/5, C/3, and 1C, again with no apparent difference in cycling performance. As seen in Fig. 2, the conductive carbon network remains on the underside of the surface-most particles even after 30 min of etching and provides the necessary electronic pathway to maintain normal performance.

EIS of the pristine and 30-min etched cathode show less than 1 Ωcm^2 in the high frequency region and only a minor increase in the cathode charge transfer resistance due to the surface etching but does not appear to significantly effect performance at normal current densities (Supporting Information, Fig. S8). Long-term cycling was carried out at a rate of C/5 and again shows no apparent difference between any of the cathode samples over the subsequent 50 cycles.

We use an abuse charging protocol to intentionally induce internal dendritic shorting (Fig. 4). A schematic of the abuse charging set up is shown in Fig. 4a, where a thermocouple is taped to the outer casing of a standard NMC/Li metal coin cell to measure temperature rise, which is then placed in a thermally insulated sheath. Fig. 4b shows an example voltage vs time trace (30-min etched, 3rd cycle). All batteries were subjected to identical conditions: pre-cycling at a rate of C/3, with a discharge to 3.5 V. The batteries were then subjected to 4.5 V potentiostatic abuse charging step for 15 min. By using a potentiostatic hold as opposed to a galvanostatic scheme, current is allowed to freely flow during the charge process. This in turn deposits highly dendritic Li on the anode surface which quickly grows to penetrate the separator and short the cell within a matter of minutes.

The potentiostatic abuse charging current profiles as well as cell temperature profiles for electrodes prepared with varying etching times are plotted in Fig. 4c. For all cathodes shorting occurred between 2 and 3 min due to an extremely high average current density $>20 \text{ mA/cm}^2$, which equates to a charging rate of greater than 10C. When internal shorting was established, the pristine cathode reached a peak current density of nearly 90 mA/cm^2 with an accompanying cell temperature rising to over 50°C . The 30-min etched cathode was limited to a short current density of 43 mA/cm^2 with the accompanying temperature remaining below 35°C . The 10-min etching current-temperature profile was similar, albeit slightly higher by about 10 mA/cm^2 than the 30-min etched. This matches previous EDS elemental C mapping and conductivity measurements. The 5-min etching, while managing to mitigate some short circuit current, is more similar to the pristine cathode, which is also in line with previous carbon content observations. Surface carbon is removed during the 5-min etch, yet enough carbon remains below the immediate surface to induce significant shorting.

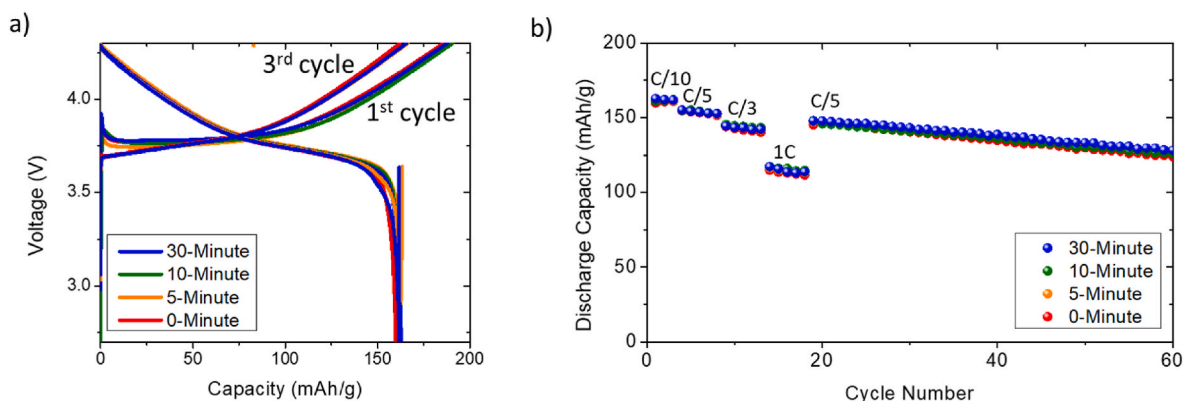


Fig. 3. a) 1st and 3rd cycle voltage profile and b) cycling stability and capacity retention at different rates for the various durations of carbon etching.

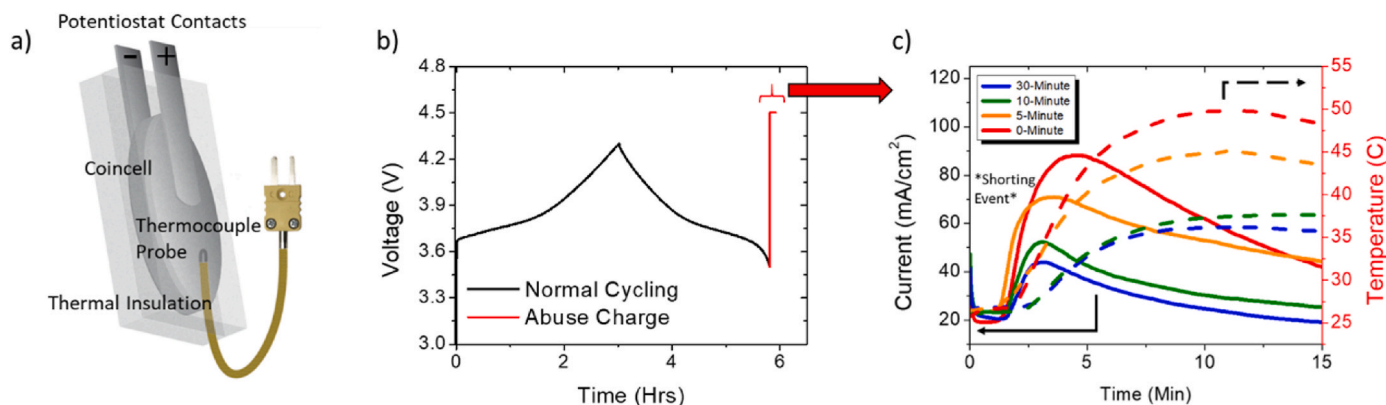


Fig. 4. Abuse shorting tests. a) Schematic of the abuse charging experimental set up where a thermocouple is attached to the outer coin cell casing, which is then placed in a thermally insulating sheath. b) Example voltage vs time profile, where cells are normally cycled to a discharge state then subjected to a 4.5 V potentiostatic abuse charging step. c) The corresponding potentiostatic abuse charging current and cell temperature profile.

2.4. Post-mortem characterization

Upon disassembling the cells after abuse shorting test, multiple dendrite contact areas were observed on the 30-min etched cathode surface (Fig. 5a). Furthermore, the pristine cathode surface shows nearly identical shorting behavior, indicating that a change in the physical mechanism of shorting was not what altered current response (Supporting Information, Fig. S9). These images show that shorting took place at multiple spots and lithium dendrites appear to grow laterally on the electrode surface. By FIB-SEM cross-section milling of the dendrite/cathode interface and observing this area at an angle (52°) the lateral

growth of these dendrites is clearly seen (Fig. 5b). Importantly, the short does not appear to penetrate into the depth of the cathode which allows the surface etching strategy to be successful. Furthermore, it is suspected that Li metal continues to deposit on the cathode surface after the short is initiated increasing the shorting area. As the effective shorting area grows, as well as new contacts are initiated, an increase in I_{SC} occurs as seen in Fig. 4c. Once the remaining capacity is expended from the cathode, short growth ceases and the current begins to decay as the highly reactive interface begins to passivate.

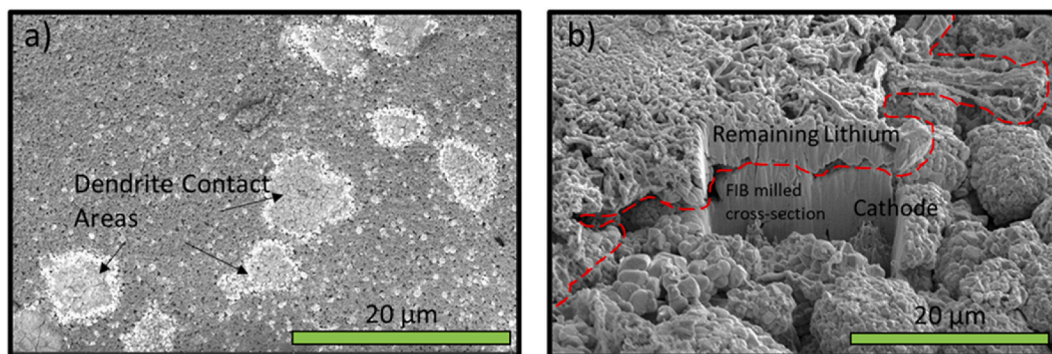


Fig. 5. Post-mortem analysis of internal shorting. a) SEM image of the 30-min etched cathode surface after abuse charging showing multiple dendrite contact areas resulting in severe shorting. b) FIB-SEM milled cross-section of the dendrite/cathode interface showing a the dendrite remains on the surface and grows laterally without penetrating into the cathode.

3. Conclusions

We have presented a new design to mitigate the impact of internal shorting in order to improve lithium battery safety. By selectively etching away the conductive carbon network only at the surface of the cathode, we create a cathode with an electronic conductivity gradient with the top layer processing reduced conductivity. Etching is limited to roughly 10 μm of depth into the cathode, and the surface-most particles remain electronically connected to the bulk via their underside. This design allows the cathode to maintain normal performance. The presence of a top layer with reduced electronic conductivity results in a significantly higher short circuit resistance which is evident during abuse charging induced shorting experiments, where optimally etched cathode had $> 2x$ reduction in short circuit current and accompanying cell temperature rise. Postmortem SEM characterization of the cathodes reveal a failure mechanism caused by growth of numerous dendritic shorts; however, these contact areas appear to only grow laterally on the cathode surface without penetrating into the bulk of the cathode. This protection scheme is applicable to any common commercial cathode tape that uses a conductive carbon network. The method is simple and scalable, without negatively impacting battery energy density. To further improve the economies of scale and create thinner carbon free layers, potential approaches are not limited to plasma etching and can include mechanical removal methods or by an additional coating step of a carbon free metal oxide skin layer easily integrated into the roll-to-roll processes that are well established for electrode fabrication.

4. Experimental section

4.1. Cathode details

The cathode is approximately 50 μm thick with a capacity of 2.2 mAh cm^{-2} and contains NMC532 ($\text{Li}_x\text{Ni}_{0.5}\text{Mn}_{0.3}\text{Co}_{0.2}\text{O}_2$), MWCNTs (multi-walled carbon nanotubes), and PVDF (Polyvinylidene fluoride) in a mass ratio of 97.5:1:1.5 on Al foil (Hunan Hong Xiang New Energy Technology CO.LTD).

4.2. Etching details

Roughly 10 cm \times 10 cm squares of the cathode tape were cut and placed into the vacuum chamber of a Ladd/Hummer™ 6.2 sputter coat machine equipped with sacrificial Al target and Ar gas. The vacuum chamber was evacuated to 80 mTorr with a steady flow of Ar and 5, 10, or 30 min of reversed polarity sputter etching was performed at a current of 10 mA to remove surface carbon.

4.3. 4-Probe measurements

Sheet resistance measurements were collected using 0.5 cm wide, 0.05 cm thick freestanding cathodes with thin strips of conductive Cu tape spaced 0.25 cm apart as electrical contacts. Various currents ranging from 1 μA to 10 mA were applied between the outer two contacts, and the voltage between the inner two was measured. This was convert to resistance, sheet resistance, and conductivity using the formula described in the main text.

4.4. Coin cell assembly, cycling, abuse shorting testing

Coin cells were assembled within an Ar atmosphere glovebox ($\text{O}_2 < 1$ ppm, $\text{H}_2\text{O} < 1$ ppm) with 2032 stainless steel casings and used 13 mm diameter cathodes paired with a 15 mm diameter Li disk rolled onto a 1 mm thick stainless steel spacer disk. 1.0 M LiPF₆ in 1:1 vol/vol ethylene carbonate (EC) and dimethyl carbonate (DMC) (LP30, Gotion) was used as the electrolyte. The cell was sealed in a hydraulic crimper at 1000 psi. Coin cells were cycled using a Landt battery tester. Coin cells the potentiostatic tests were precycled at a rate of C/10 for the first cycle

and C/3 for the following two cycles (3rd cycle cut-off was set to 3.5 V). Potentiostatic holds and impedance measurements were carried with a Biologic potentiostat using a high current (10 A, 5 V) booster channel. Temperature was measured using a K-type thermocouple and HOBOware reader.

4.5. XPS characterization

XPS spectra (Supporting Information, Fig. S7) used to calculate the doping level of ion gate material was performed by a PHI Quantera SXM, Scanning X-ray Microprobe and was carried out using Al anode source at 15 kV and all the peaks were fitted based on the reference C-C bond at 284.6 eV. All XPS measurements were collected with a 300 mm \times 700 mm spot size using a charge neutralizer during acquisition. Survey scans were collected with a 1.0 eV step size, and were followed by high resolution scans with a step size of 0.05 eV for Ni2p, Co2p, and Mn2p regions.

CRediT authorship contribution statement

Matthew S. Gonzalez: Conceptualization, Methodology, Validation, Investigation, Visualization, Writing – original draft. **Zhaohui Wu:** Methodology, Resources. **John Holoubek:** Conceptualization, Writing – review & editing. **Qizhang Yan:** Conceptualization. **Haodong Liu:** Conceptualization, Writing – review & editing, Project administration. **Ping Liu:** Conceptualization, Writing – review & editing, Supervision, Project administration.

Declaration of competing interest

The authors declare that they have no known competing financial interests or personal relationships that could have appeared to influence the work reported in this paper.

Acknowledgements

P.L. proposed the idea and directed the research along with H.L. All of the authors contributed to the planning, materials fabrication, experimental design and analysis, and manuscript preparation. M.S.G. performed the majority of separator fabrication and characterization as well as cell fabrication, and electrochemical testing. Z.W. and Q.Y. aided in characterization and cell design. J.H. helped in experimental design and analyzing results. The majority of cell fabrication and electrochemical testing was performed in the UCSD-MTI Battery Fabrication and the UCSD-Arbin Battery Testing Facility. We acknowledge Hunan Hong Xiang New Energy Technology CO.LTD for supplying high capacity NMC cathode tapes.

Appendix A. Supplementary data

Supplementary data to this article can be found online at <https://doi.org/10.1016/j.jpowsour.2021.230412>.

References

- [1] P.M. Halmo, X. Zhang, P.D. Vido, Z. Zhang, L. Shi, D.R. Alexander, J.V. Watson, *Thin Battery Separators and Methods*, 2017. US9666847B2.
- [2] M. Singh, J. Kaiser, H. Hahn, *J. Electrochem. Soc.* 162 (2015) A1196.
- [3] P. Li, G. Zhao, X. Zheng, X. Xu, C. Yao, W. Sun, S.X. Dou, *Energy Storage Mater.* 15 (2018) 422.
- [4] X.-B. Cheng, R. Zhang, C.-Z. Zhao, Q. Zhang, *Chem. Rev.* 117 (2017) 10403.
- [5] K. Liu, Y. Liu, D. Lin, A. Pei, Y. Cui, *Sci. Adv.* 4 (2018), eaas9820.
- [6] D. Ouyang, M. Chen, J. Liu, R. Wei, J. Weng, J. Wang, *RSC Adv.* 8 (2018) 33414.
- [7] B. Liu, Y. Jia, J. Li, S. Yin, C. Yuan, Z. Hu, L. Wang, Y. Li, J. Xu, *J. Mater. Chem. A* 6 (2018) 21475.
- [8] H. Maleki, J.N. Howard, *J. Power Sources* 191 (2009) 568.
- [9] P. Ghosh, Hyundai to recall 76,000 electric vehicles over battery fire risks, can be found under, <https://www.forbes.com/sites/palashghosh/2021/02/24/hyundai-to-recall-76000-electric-vehicles-over-battery-fire-risks/>. (Accessed April 2021).

- [10] Global automotive lithium ion battery pack market size & forecast 2025 - valuates reports, can be found under, <https://reports.valuates.com/market-reports/QYRE-Auto-0U1490/global-automotive-lithium-ion-battery>. (Accessed March 2021).
- [11] Q. Wang, P. Ping, X. Zhao, G. Chu, J. Sun, C. Chen, *J. Power Sources* 208 (2012) 210.
- [12] W. Na, A.S. Lee, J.H. Lee, S.S. Hwang, E. Kim, S.M. Hong, C.M. Koo, *ACS Appl. Mater. Interfaces* 8 (2016) 12852.
- [13] W. Yi, Z. Huaiyu, H. Jian, L. Yun, Z. Shushu, *J. Power Sources* 189 (2009) 616.
- [14] A. Gogia, Y. Wang, A.K. Rai, R. Bhattacharya, G. Subramanyam, J. Kumar, *ACS Omega* 6 (2021) 4204.
- [15] C. Shi, J. Dai, X. Shen, L. Peng, C. Li, X. Wang, P. Zhang, J. Zhao, *J. Membr. Sci.* 517 (2016) 91.
- [16] K. Liu, D. Zhuo, H.-W. Lee, W. Liu, D. Lin, Y. Lu, Y. Cui, *Adv. Mater.* 29 (2017), 1603987.
- [17] H. Wu, D. Zhuo, D. Kong, Y. Cui, *Nat. Commun.* 5 (2014) 5193.
- [18] L. Kong, B. Liu, J. Ding, X. Yan, G. Tian, S. Qi, D. Wu, *J. Membr. Sci.* 549 (2018) 244.
- [19] M. Naguib, S. Allu, S. Simunovic, J. Li, H. Wang, N.J. Dudney, *Joule* 2 (2018) 155.
- [20] Z. Chen, P.-C. Hsu, J. Lopez, Y. Li, J.W.F. To, N. Liu, C. Wang, S.C. Andrews, J. Liu, Y. Cui, Z. Bao, *Nat. Energy* 1 (2016) 1.
- [21] X.M. Feng, X.P. Ai, H.X. Yang, *Electrochem. Commun.* 6 (2004) 1021.
- [22] H. Zhong, C. Kong, H. Zhan, C. Zhan, Y. Zhou, *J. Power Sources* 216 (2012) 273.
- [23] M.S. Gonzalez, Q. Yan, J. Holoubek, Z. Wu, H. Zhou, N. Patterson, V. Petrova, H. Liu, P. Liu, *Adv. Mater.* 32 (2020), 1906836.
- [24] K. Dokko, M. Mohamedi, Y. Fujita, T. Itoh, M. Nishizawa, M. Umeda, I. Uchida, *Electrochem. Soc.* 148 (2001) A422.
- [25] M.M. Thackeray, *Prog. Solid State Chem.* 25 (1997) 1.
- [26] P.P. Prossini, M. Lisi, D. Zane, M. Pasquali, *Solid State Ionics* 148 (2002) 45.
- [27] Y. Itou, N. Ogihara, S. Kawauchi, *J. Phys. Chem. C* 124 (2020) 5559.
- [28] R. Benedek, J. Vaughey, M.M. Thackeray, *Chem. Mater.* 18 (2006) 1296.
- [29] L. Yu, Y. Tian, X. Xiao, C. Hou, Y. Xing, Y. Si, H. Lu, Y. Zhao, *J. Electrochem. Soc.* 168 (2021), 050516.
- [30] A.P. Grosvenor, M.C. Biesinger, R. St, C. Smart, N.S. McIntyre, *Surf. Sci.* 600 (2006) 1771.
- [31] L. Baggetto, N.J. Dudney, G.M. Veith, *Electrochim. Acta* 90 (2013) 135.
- [32] J.C. Dupin, D. Gonbeau, H. Benqlilou-Moudden, P. Vinatier, A. Levasseur, *Thin Solid Films* 384 (2001) 23.
- [33] S.J. Pearton, D.P. Norton, *Plasma Process. Polym.* 2 (2005) 16.